BMB
Reports

Dual positional substrate specificity of rice allene oxide synthase-1: insight into mechanism of inhibition by type II ligand imidazole

Sereyvath Yoeun[1], *Randeep Rakwal*[2] *& Oksoo Han*[1,*]

[1]Department of Molecular Biotechnology and Kumho Life Science Laboratory, College of Agriculture and Life Sciences, Chonnam National University, Gwangju 500-757, Korea, [2]Health Technology Research Center (HTRC), National Institute of Advanced Industrial Science and Technology (AIST), Tsukuba 305-8569, Japan

Phylogenetic and amino acid sequence analysis indicated that rice allene oxide synthase-1 (OsAOS1) is CYP74, and is clearly distinct from CYP74B, C and D subfamilies. Regio- and stereo-chemical analysis revealed the dual substrate specificity of OsAOS1 for (cis,trans)-configurational isomers of 13(S)- and 9(S)-hydroperoxyoctadecadienoic acid. GC-MS analysis showed that OsAOS1 converts 13(S)- and 9(S)-hydroperoxyoctadecadi(tri)enoic acid into their corresponding allene oxide. UV-Visible spectral analysis of native OsAOS1 revealed a Soret maximum at 393 nm, which shifted to 424 nm with several clean isobestic points upon binding of OsAOS1 to imidazole. The spectral shift induced by imidazole correlated with inhibition of OsAOS1 activity, implying that imidazole may coordinate to ferric heme iron, triggering a heme-iron transition from high spin state to low spin state. The implications and significance of a putative type II ligand-induced spin state transition in OsAOS1 are discussed. [BMB Reports 2013; 46(3): 151-156]

INTRODUCTION

Oxylipins are produced by oxidative metabolism of polyunsaturated fatty acids and play diverse roles in host defense in plants and animals (1). In plants, the biosynthesis of oxylipins is initiated by lipoxygenase (LOX), which oxygenates linoleic acid (LA) or linolenic acid (LnA) at the C-9 or C-13 position to produce fatty acid hydroperoxides (2). Allene oxide synthase (AOS) converts fatty acid hydroperoxides into unstable fatty acid epoxides (allene oxides) (3). The AOS branch of the 13-LOX pathway (4, 5) has been studied extensively in biosynthesis of jasmonic acid (JA). In particular, 13-AOS converts 13(S)-hydroperoxyoctadecatrienoic acid (13(S)-HPOTE), produced by 13-LOX, to the corresponding allene oxide, 12,13-epoxy-9,11,15-octadecatrienoic acid (12,13-EOT) (6, 7). The allene oxide is then metabolized to 12-oxophytodienoic acid (12-OPDA) by allene oxide cyclase (AOC), which subsequently undergoes reduction and β-oxidation to yield JA (8-10).

AOS is a non-classical cytochrome P450, which, like other CYP74 enzymes, does not require molecular oxygen and NADPH-dependent P450 reductase (11). Instead, CYP74 family enzymes use a hydroperoxide group both as the activated oxygen donor and as a source of reducing equivalents (12). AOS exemplifies the unique structural and mechanistic features that distinguish CYP74 enzymes from classical cytochrome P450. Most AOS enzymes of plants strongly prefer 13-hydroperoxy fatty acids over 9-hydroperoxy fatty acids (13). However, AOS from *ArabiHdopsis* (14), tomato (15), and barley (16) metabolize both 9-HPOD(T)E and 13-HPOD(T)E *in vitro* and metabolites of 9-AOS have been identified *in vivo*. Despite the importance of the 9-LOX/AOS pathway, the physiological significance of the 9-positional substrate specificity of AOS is not known. Sequence alignments and X-ray crystal structures clearly show that the heme-binding region of AOS contains a characteristic heme loop which is not present in classical cytochrome P450s (17). The heme environment is an important determinant of the spin states of heme-chelated iron in P450 (18). ESR studies show that recombinant *Arabidopsis* AOS contains both low and high spin states (14), and the UV-visible spectrum of purified flaxseed AOS indicates that ferric iron is in the high spin state (19). In classical cytochrome P450s, type I ligands stabilize the high spin state by displacing the water molecule liganded to heme iron(III), while in contrast, type II ligands (nitrogen-containing ligands) replace the water ligand, but stabilize the low spin state (20). However, the spectral behavior of dual positional specific AOS in the presence of type II ligands has never been analyzed.

Rice (*Oryza sativa*) is considered as a model monocot for

*Corresponding author. Tel: +82-62-530-2163; Fax: +82-62-530-2049; E-mail: oshan@chonnam.ac.kr
http://dx.doi.org/10.5483/BMBRep.2013.46.3.117

Received 1 June 2012, Revised 19 September 2012, Accepted 24 September 2012

Keywords: Allene oxide synthase, Cytochrome P450, Enzyme, Lipid, Octadecanoid

ISSN: 1976-6696 (print edition) / 1976-670X (electronic edition)

Table 1. Kinetic parameters and comparison of AOS[a] and HPL activity of OsAOS1

Substrate	K_m (μM)	k_{cat} (s^{-1})	k_{cat}/K_m (M^{-1} s^{-1})	Relative specific activities (%)	
				AOS activity	HPL activity
13(S)-HPODE	12.5 (15.0 ± 7.2[b])	494.5 (108 ± 21[b])	39.6×10^6	91.4 (80[c])	8.6 (15[c])
13(S)-HPOTE	12.3	537.8	43.7×10^6	98.2 (81[c])	1.8 (12[c])
9(S)-HPODE	6.9	44.9	6.5×10^6	90.3	9.7
9(S)-HPOTE	8.6	17.5	2.0×10^6	98.4	1.6

[a]AOS activity was estimated by subtraction of the HPL activity from the total rate of substrate consumption. [b]Ref 11. [c]Determined by the end point product quantification method (30).

studying and understanding plant host defense systems. The rice genome encodes at least five AOS variants (AOS1 to AOS5) (21). We previously showed that *O. sativa AOS1* (OsAOS1 known as OsAOS) is expressed in various tissues and is induced by JA, heavy metals, pathogen attack, and protein phosphatase inhibitors (22, 23), suggesting that OsAOS1 plays an important role in host defense/stress response. Here, we characterized the kinetic properties of OsAOS1, identified the reaction products generated by OsAOS1 from 13(S)-HPOD(T)E or 9(S)-HPOD(T)E, and examined the effect of type II ligands on the spectral shift of the Soret band and possible spin state transition.

RESULTS

Kinetic parameters and specificity of OsAOS1

The kinetic parameters of OsAOS1 with 9- and 13-positional isomers of HPOD(T)E were measured, and the results are shown in Table 1. K_m and k_{cat} for 13(S)-HPOD(T)E were larger than for 9(S)-HPOD(T)E, and catalytic efficiency (k_{cat}/K_m) was 6- or 20-times higher for 13-positional isomers of HPODE or HPOTE, respectively, than for the corresponding 9-positional isomers. Therefore, OsAOS1 exhibits dual positional substrate specificity and prefers 13-positional isomeric to 9-positional isomeric substrates *in vitro*. AOS enzymes also convert hydroperoxy fatty acids to aldehydes *via* an HPL-like activity. As shown in Table 1, the HPL-like activity of OsAOS1 was a minor pathway with 9- and 13-positional isomers of HPODE as a substrate, and the 9- and 13-positional isomers of HPOTE were utilized only for the AOS pathway.

In order to analyze regiochemical and stereochemical specificity of OsAOS1, a racemic mixture of four regioisomers of HPODE was generated by dual positional specific maize LOX1 (ZmLOX1) (24, 25), and OsAOS1 was added to an aliquot of this reaction. Reaction products were extracted and were analyzed by normal phase HPLC. Fig. 1A shows that the products of ZmLOX1 are a racemic mixture of four regioisomers of HPODE (13-(9Z,11E)-(HPODE) (I); 13-(9E,11E)-HPODE (II); 9-(10E,12Z)-HPODE (III); 9-(10E,12E)-HPODE) (IV). Fig. 1B showed that the relative proportion of regioisomers I and III was rapidly decreased to 50% after addition of OsAOS1, which indicates dual positional substrate specificity and implies stereospecificity of OsAOS1 reaction. The relative ratios of the 4 regioisomers in Fig. 1A (absence of OsAOS1) and 1B (presence of OsAOS1) were quantified and compared in Fig. 1C. These data confirmed that OsAOS1 prefers regioisomers I and III as substrates. Chiral phase HPLC analysis further confirmed the S-stereospecificity of OsAOS1 (insets of Fig. 1A and B). Therefore, OsAOS1 is dual positional substrate specific and stereospecific for (cis, trans)-configurational isomers of 9(S)- HPODE and 13(S)-HPODE. However, our results in Fig. 1 also indicate that the S form of regioisomer II is consumed in a very slow and minor reaction pathway. This might be due to the broad substrate specificity required

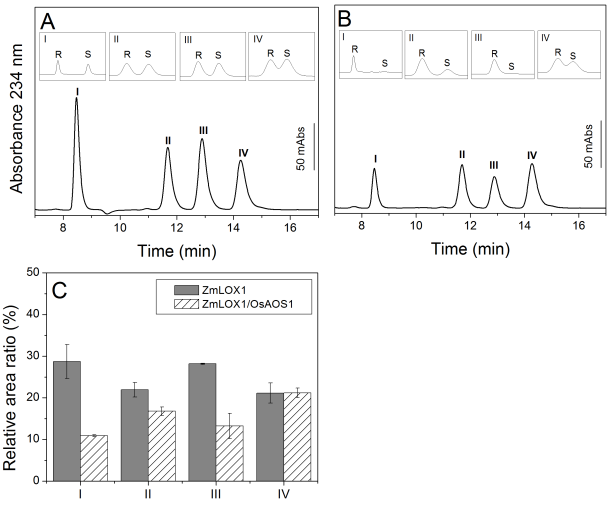

Fig. 1. Determination of positional substrate specificity and stereospecificity of OsAOS1 by dual positional specific ZmLOX1. (A) Normal phase HPLC chromatogram from dual positional specific ZmLOX1 reaction (I, 13-(9Z,11E)-(HODE); II, 13-(9E,11E)-HODE; III, 9-(10E,12Z)-HODE; IV, 9-(10E,12E)-HODE). (B) Normal phase HPLC chromatogram showing remaining regioisomers after OsAOS1 was added to ZmLOX1 reaction mixture, (C) The relative ratios of four regioisomers from (A) and (B). The stereochemistry of each regioisomer was further analyzed by chiral phase HPLC, as shown in insets of (A) and (B).

for the dual positional specificity of OsAOS1.

Identification of OsAOS1 reaction products

To confirm the assumption that OsAOS1 produces the expected allene oxides, normal phase HPLC analysis was carried out on the reaction products. As shown in Fig. 2, the single major product generated from 13(S)-HPODE was tentatively assigned as an 13α-ketol (Fig. 2A) and the two major products generated from 13(S)-HPOTE as 13α-ketol(15en) and cis-OPDA (Fig. 2B). In contrast, a single major peak was generated from 9(S)-HPODE or 9(S)-HPOTE, that was tentatively identified as an 9α-ketols (Fig. 2C and D). Therefore, a major putative non-enzymatic cyclization product was generated from 13(S)-HPOTE, while minor putative cyclization products were generated from13(S)-HPODE and 9(S)-HPOD(T)E.

To identify the structures of products generated by OsAOS1 from 13(S)-HPOD(T)E, putative α-ketols and cis-OPE(D)A were derivatized with TMSiCl and analyzed by GC-MS, which yielded at least two products from each substrate (Fig. S2A-D): 13α-ketol (13-hydroxy-12-oxo-9(Z)-octadecenoic acid) and 12-OPEA (12-oxo-10-phytoenoic acid) from 13(S)-HPODE, whereas 13α-ketol(15en) (13-hydroxy-12-oxo-9(Z),15(Z)-octadecadienoic acid) and 12-OPDA (12-oxo-10,15(Z)-phytodienoic acid) were identified from 13(S)-HPOTE. These data show that OsAOS1 produced cis-12-OPDA as one of two major products from 13(S)-HPOTE. The stereochemistry of cis-12-OPDA generated by OsAOS1 was analyzed by chiral phase HPLC. As expected, the inset of Fig. 2B shows that OsAOS1 produced a 1 : 1 racemic mixture of cis-(+)/cis-(-)-12-OPDA *via* non-enzymatic cyclization of 12,13-EOT. Therefore, HPLC and GC-MS analysis clearly showed that OsAOS1 converts 13(S)-HPOD(T)E into the unstable allene oxide (12,13-EOD(T)), which is rapidly converted into corresponding 13α-ketols and racemic 12-OPE(D)A.

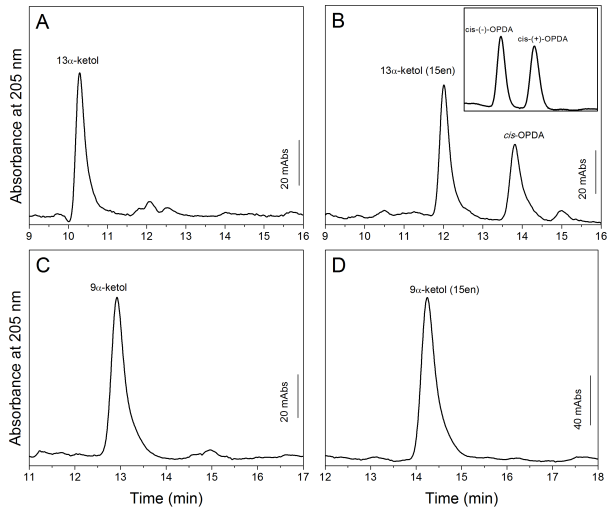

Fig. 2. HPLC analysis of OsAOS1 reaction products. (A) 13(S)-HPODE as a substrate. (B) 13(S)-HPOTE as a substrate. The chiral phase HPLC chromatogram of cis-OPDA is shown in the inset. (C) 9(S)-HPODE as a substrate. (D) 9(S)-HPOTE as a substrate.

Using normal phase HPLC, only one major reaction product was detected from reaction with OsAOS1 and 9(S)-HPOD(T)E. Other minor products produced by OsAOS1 from 9(S)-HPOD(T)E were characterized by GC-MS after reaction products were methylated with (trimethylsilyl) diazomethane prior to being derivatized with TMSiCl (Fig. S3A-G). GC-MS analysis identified the following products; 9α-ketol (Fig. S3A), 13γ-ketol (Fig. S3C) and 10-OPEA (Fig. S3E) presumably derived from 9(S)-HPODE through 9,10-EOD, and 9α-ketol(15en) (Fig. S3B), 13γ-ketol(15en) (Fig. S3D) and 10-OPDA (Fig. S3F) derived from 9(S)-HPOTE through 9,10-EOT. In addition, OsAOS1 also generated 9-oxo-nonanoic acid from 9(S)- HPOD(T)E, the expected product of the HPL-like activity of OsAOS1 (Fig. S3G). These data show that OsAOS1 converts 9(S)-HPODE or 9(S)-HPOTE into the corresponding unstable allene oxides, 9,10-EOD or 9,10-EOT, respectively, which are non-enzymatically transformed into a 9α-ketol as the major product, and 13γ-ketols and cyclopentenone derivatives as minor products.

Spectral characterization and shift of Soret bands induced by type II ligands

The UV-visible spectrum of native oxidized OsAOS1 showed a Soret maximum at 393 nm and major broad spectral features at 520 nm and 650 nm (Fig. 3), consistent with a high spin state of OsAOS1 (18, 19). Reduction of OsAOS1 with sodium

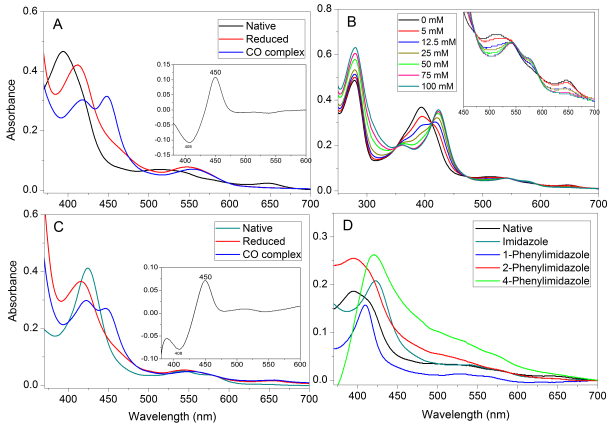

Fig. 3. UV-Visible and spectral shift of OsAOS1 by imidazole. (A) Visible spectra of native (black), reduced (red), carbon monoxide-treated (blue) OsAOS1. (B) Dose-dependent spectral shift of native OsAOS1 in response to imidazole. Concentrations of imidazole were shown in inset of (B). (C) Visible spectra of native (dark cyan), reduced (red), carbon monoxide-treated (blue) OsAOS1 complexed with imidazole. The inset in (A, C) shows the difference spectra obtained by subtracting the reduced form from the carbon monoxide-treated reduced form of OsAOS1. (D) Comparison of spectral shifts of native OsAOS1 by imidazole derivatives. The spectra in (D) were obtained with OsAOS1 containing 100 mM of imidazole derivatives and 30% ethanol.

dithionite shifted the absorption maximum to 412 nm, and after bubbling carbon monoxide through a solution of reduced OsAOS1, absorption maxima were detected at 418 nm and 448 nm (Fig. 3A). The carbon monoxide difference spectrum of OsAOS1 showed an absorption maximum at 450 nm, which is typical for cytochrome P450s (inset Fig. 3A).

Imidazole, a well-known type II ligand of classical P450s (26), was tested as an external ligand for OsAOS1 heme, and possible alterations of the spectral properties were examined. As shown in Fig. 3B, imidazole induced characteristic gradual concentration-dependent changes in the UV-visible spectrum of OsAOS1. In particular, the Soret maximum at 393 nm decreased and absorbance at 424 nm increased, with clean isosbestic points at 412 nm, 472 nm, 545 nm, 592 nm (inset of Fig. 3B), which implied a putative spin state transition. However, imidazole did not affect the spectrum of reduced OsAOS1 or the shape of the carbon monoxide difference spectra as seen in Fig. 3C. Similar spectral shifts were observed with other type II ligands, and the magnitude of the spectral shift correlated with the size and predicted severity of steric hindrance by the ligand (Fig. 3D). These data show that imidazole binds to OsAOS1 as an external type II ligand, and induces a shift of the Soret band characteristic for spin state transition of heme-associated ferric iron(III).

To further characterize imidazole-bound OsAOS1, Scatchard analysis was performed on OsAOS1 with imidazole as a ligand. As shown in Fig. S4A, the dissociation constant (K_d) of the OsAOS1-imidazole complex was 15.3 mM. Therefore, binding of imidazole to OsAOS1 may induce a change in heme-iron spin state from high to low, and the AOS activity is predicted to be decreased due to the unfavorable spin state. Indeed, Fig. S4B shows that the AOS activity of OsAOS1 decreased in the presence of imidazole and confirmed this prediction

DISCUSSION

We previously reported that transcription of the OsAOS1 gene is stimulated by JA, heavy metals, and pathogen attack (22, 23), suggesting that OsAOS1 is up-regulated by biological and environmental stress, and that it may play a role in plant host-defense. Sequence analysis confirmed that OsAOS1 lacks a putative chloroplast targeting sequence, but that the small hydrophobic amino acid residue (Leu-286), characteristic of the I-helix region in CYP74 enzymes, is conserved, as is the phenylalanine residue (Phe-92) that distinguishes AOS from HPL (11) (Fig. S1B). Kinetic parameters (Table 1), the regiochemical and stereochemical positional substrate specificity (Fig. 1), and the reaction products (Fig. S2 and S3) indicate that OsAOS1 has broad substrate specificity. However, detailed analysis of the regiochemical specificity of OsAOS1 indicates a strict requirement for (cis, trans) configuration and S-stereochemistry and preference for 13-regioisomers over corresponding 9-regioisomers. Because OsAOS1 does not contain a chloroplast-targeting sequence and was detected in leaf, root, shoot, scutellum and flower of the rice plant (23), OsAOS1 could be involved in biochemical pathways other than biosynthesis of JA. The dual positional substrate specificity of OsAOS1 also suggests that it may have more than one biological function. Quantitative HPLC analysis (Fig. 2) confirmed that non-enzymatic cyclization of OsAOS1 reaction products is favored only for 12,13-EOT. As OsAOS1 only generates trace amounts of 12-OPEA and 10-OPE(D)A from 13(S)-HPODE (Fig. 2A) and 9(S)-HPOD(T)E (Fig. 2C, D), two homoallylic double bonds on either side of the allene oxide epoxide ring (as in 12,13-EOT) may be required for effective cyclization into a cyclopentenone derivative as observed for allene oxide cyclase (27). If this is the case, the AOS pathway is expected to be more favorable with HPOTE than with HPODE. Relative AOS and HPL specific activities indicate that the HPL-like activity of OsAOS1 is a minor sub-pathway, generating a trace amount of HPL product from 9(S)-HPOTE or 13(S)-HPOTE (Table 1). Because 13(S)-HPOTE is a precursor of JA, but 13(S)-HPODE is not, it is likely that OsAOS1 is involved in JA signaling (23) and plays an important role in defense/stress responses of rice (22).

Cytochrome P450 enzymes have a characteristic UV visible absorption profile that varies according to the heme spin state. Spectral features of native OsAOS1 in Fig. 3 suggest that ferric iron in native OsAOS1 assumes predominantly the high spin state (18, 19). Here, we show that the OsAOS1 Soret band shifts to 424 nm when type II ligands are bound (Fig. 3B). It is well known that nitrogen-containing type II ligands can replace the water ligand in P450 and shift the iron(III) spin equilibrium from high to low (20). This suggests that coordination of imidazole to ferric heme iron(III) of OsAOS1 induces a drastic spectral shift, and that a comparable shift towards a low spin state occurs (28). Thus, our results support the idea that imidazole coordinates as the sixth ligand to the pentacoordinated OsAOS1 heme iron(III) in high spin state, and that hexacoordinated heme iron(III) adopts the low spin state in native OsAOS1. Detailed EPR studies of the spin states of OsAOS1 are required to confirm this possibility. In this respect, OsAOS1 may be a useful model for understanding spin transitions induced by type II ligands in non-classical cytochrome P450s. If type II ligands directly coordinate with the heme iron of native OsAOS1, the binding of carbon monoxide to reduced OsAOS1 may also be influenced. However, as seen in Fig. 3C, imidazole did not change the absorption maximum of reduced OsAOS1, and its carbon monoxide difference spectrum was identical in the presence and absence of imidazole. This likely reflects the fact that imidazole is a weaker ligand for inorganic iron than carbon monoxide, and thus would not be able to displace carbon monoxide from reduced OsAOS1. Consistent with this, a relatively high concentration of imidazole is needed for binding to OsAOS1 (K_d = 15.3 mM). Because cytochrome P450 is more active in the high spin state than in the low spin state (20), imidazole is expected to inhibit OsAOS1 activity as confirmed in Fig. S4B. This suggests that imidazole inhibits OsAOS1, as it promotes transition from

high spin state to low spin state. Previous studies reported that positional substrate specificity depends on the spin state of AOS. For example, 13-AOS from flax seed was in high spin (19), 9-AOS from tomato was in low spin (15), and the dual positional substrate specific AOS from *Arabidopsis* contained a mixture of high and low spin ferric heme iron in its resting form (14). Therefore, OsAOS1 is an ideal system to investigate the relationships between spectral shift, spin state transition and positional substrate specificity of CYP74 in detail.

MATERIALS AND METHODS

Expression and purification of recombinant OsAOS1

An expression vector containing the OsAOS1 gene was constructed, and OsAOS1 protein was expressed as reported previously (23). The cells were grown, harvested by centrifugation, and disrupted by sonication in buffer (50 mM sodium phosphate, 50 U DNase, 0.2 mM PMSF, pH 7.5) containing 5 mM Emulphogene or 0.2% Tween-20. The lysate was then centrifuged at 17,000 g for 1 h and the resulting soluble fraction was applied to a Q-sepharose column. The OsAOS1 protein was subsequently eluted with buffer (50 mM sodium phosphate, pH 7.5) containing 5 mM Emulphogene.

Enzyme assay and kinetic parameters

AOS activity was measured by coupling the OsAOS1 reaction with soybean LOX or CaLOX1 reaction as reported previously (23). The kinetic constants (K_m and k_{cat}) were calculated from a Lineweaver-Burk plot. HPL activity was measured using a modification of a previously reported method (29). Excess alcohol dehydrogenase (ADH) and NADH were added to the standard assay mixture, and HPL activity was measured by monitoring decreasing absorbance at 340 nm, reflecting the decreasing concentration of NADH. HPL activity was calculated based on the assumption that two molar equivalents of aldehyde are produced from one mole hydroperoxide.

Regiochemical and stereochemical analysis of OsAOS1 reaction

The OsAOS1 reaction was coupled to that of dual positional specific ZmLOX1 (25) using LA as a substrate as follows. Purified ZmLOX1 (72 μg) was incubated in 50 mM Tris-HCl (pH 7.2) containing 0.5 mM LA and 0.05% Tween 20 (v/v) for 15 min at room temperature in a final volume of 2.5 ml. Purified recombinant OsAOS1 (114 μg) was then immediately added to the reaction, after which the enzymatic reaction was allowed to proceed for 5 min at room temperature. ZmLOX1 or ZmLOX1/OsAOS1 reaction products were extracted and were analyzed by normal phase and chiral phase HPLC as described previously (24, 25).

Structural analysis of OsAOS1 reaction products

OsAOS1 (3 μg) was added to a solution containing 0.25 mM LA (or LnA), 2 μg soybean LOX or pepper LOX, and 50 mM sodium phosphate (pH 7.5) in a total volume of 2 ml, after which the reaction was incubated at room temperature for 20 min. The reaction was then stopped by acidification with 3 M HCl to pH 3.0. The reaction mixture was extracted twice with 5 ml dichloromethane, and the combined fractions were concentrated by evaporation. The recovered reaction products were then analyzed by normal phase HPLC (Mightysil Si-60, 4.6 × 250 mm, 5 μm, Kanto Chem. Co., Japan) using a solvent system of hexane: 2-propanol: acetic acid (100 : 2 : 0.1) and a flow rate of 1 ml per minute. Two wavelengths (205 nm and 220 nm) were monitored for ketols and cyclopentenone derivatives. The cyclopentenone derivative fractions were subjected to chiral phase HPLC analysis (Chiralcel OD-H, 4.6 × 250 mm, Daicel Chemical Industries, Japan) using a solvent system of hexane: 2-propanol: acetic acid (100 : 5 : 0.1) and a flow rate 0.5 ml per minute for stereochemical analysis. Standard cis-(+)-OPDA (Cayman Chemical, USA) was co-chromatographed as a standard. Products (ketols and cyclopentanone derivatives) of 13-Soybean LOX/OsAOS1 reaction collected from normal phase HPLC were derivatized with Sigma-Sil-A (Sigma, USA) at 80°C for 5 min. Products from CaLOX1/OsAOS1 reaction were initially methylated with (trimethylsilyl)diazomethane, and/or then derivatized with TMSiCl. Methylated and/or trimethylsilylated products were then analyzed by GC-MS (Elite-5MS, 0.25 mm × 30 m, 0.25 μm film thickness, Perkin Elmer, USA) with an injector temperature of 260°C. Products were subjected to an initial temperature of 120°C for 1 min, after which the temperature was increased at 10°C/min to 280°C, where it was held for 3 min.

UV-Visible spectra of OsAOS1 in the presence and absence of type II ligands

OsAOS1 was dissolved in 50 mM sodium phosphate (pH 7.5) containing detergent. Native oxidized OsAOS1 was reduced with sodium dithionite and bubbled with carbon monoxide to produce the carbon monoxide complex of OsAOS1 in the presence or absence of imidazole. Spectra were analyzed in the presence of 0-100 mM imidazole or 100 mM imidazole derivatives including 1-, 2-, and 4-phenylimidazole. The dissociation constant of the OsAOS1-imidazole complex was determined by Scatchard analysis using molar extinction coefficients of ε_{393} = 50,242 $M^{-1}cm^{-1}$ or ε_{424} = 48,608 $M^{-1}cm^{-1}$ for OsAOS1 or the OsAOS1-imidazole complex, respectively.

Acknowledgements

This work was supported by a Korea Research Foundation grant (2008-313-F00020) to O. Han. The authors wish to thank Professor B. Hwang for providing pepper LOX (pET28a:: CaLOX1) plasmid.

REFERENCES

1. Brash, A. R. (1999) Lipoxygenases: occurrence, functions, catalysis, and acquisition of substrate. *J. Biol. Chem.* **274**,

23679-23682.
2. Siedow, J. N. (1991) Plant lipoxygenases: structure and function. *Annu. Rev. Plant. Physiol. Plant. Mol. Biol.* **42**, 145-188.
3. Veldink, G. A., Vliegenthart, J. F. G. and Boldingh, J. (1970) The enzymatic conversion of linoleic acid hydroperoxide by flax-seed hydroperoxide isomerase. *Biochem. J.* **120**, 55-60.
4. Hamberg, M. and Gardner, H. W. (1992) Oxylipin pathway to jasmonates: biochemistry and biological significance. *Biochim. Biophys. Acta.* **1165**, 1-18.
5. Grechkin, A. (1998) Recent development in biochemistry of the plant lipoxygenase pathway. *Prog. Lipid Res.* **37**, 317-352.
6. Grechkin, A. N., Mukhtarova, L. S., Latypova, L. R., Gogolev, Y., Toporkova, Y. Y. and Hamberg, M. (2008) Tomato CYP74C3 is a multifunctional enzyme not only synthesizing allene oxide but also catalyzing its hydrolysis and cyclization. *Chembiochem.* **9**, 2498-2505.
7. Hughes, R. K., De Domenico, S. and Santino, A. (2009) Plant cytochrome CYP74 family: biochemical features, endocellular localization, activation mechanism in plant defense and improvements for industrial applications. *Chembiochem.* **10**, 1122-1133.
8. Mueller, M. J. (1997) Enzymes involved in jasmonic acid biosynthesis. *Physiol. Plant.* **100**, 653-663.
9. Beale, M. H. and Ward, J. L. (1998) Jasmonates: key players in the plant defense. *Nat. Prod. Rep.* **15**, 533-548.
10. Schaller, F. (2001) Enzymes of the biosynthesis of octadecanoid-derived signaling molecules. *J. Exp. Bot.* **52**, 11-23.
11. Lee, D. S., Nioche, P., Hamberg, M. and Raman, C. S. (2008) Structural insights into the evolutionary paths of oxylipin biosynthetic enzymes. *Nature* **455**, 363-368.
12. Song, W. C., Funk, C. D. and Brash, A. R. (1993) Molecular cloning of an allene oxide synthase: A cytochrome P450 specialized for the metabolism of fatty acid hydroperoxides. *Proc. Natl. Acad. Sci. U.S.A.* **90**, 8519-8523.
13. Howe, G. A., Lee, G. I., Itoh, A., Li, L. and De Rocher, A. E. (2000) Cytochrome P450-dependent metabolism of oxylipins in tomato: cloning and expression of allene oxide synthase and fatty acid hydroperoxide lyase. *Plant Physiol.* **123**, 711-724.
14. Hughes, R. K., Belfield, E. J., Ashton, R., Fairhurst, S. A., Göbel, C., Stumpe, M., Feussner, I. and Casey, R. (2006) Allene oxide synthase from Arabidopsis thaliana (CYP74A1) exhibits dual specificity that is regulated by monomer-micelle association. *FEBS Letters* **580**, 4188-4194.
15. Itoh, A., Schilmiller, A. L., McCaig, B. C. and Howe, G. A. (2002) Identification of a jasmonate-regulated allene oxide synthase that metabolizes 9-hydroperoxides of linoleic and linolenic acids. *J. Biol. Chem.* **277**, 46051-46058.
16. Maucher, H., Hause, B., Feussner, I., Ziegler, J. and Wasternack, C. (2000) Allene oxide synthases of barley (Hordeum vulgare cv. Salome): tissue specific regulation in seedling development. *Plant J.* **21**, 199-213.
17. Brash, A. R. (2009) Mechanistic aspects of CYP74 allene oxide synthases and related P450 enzymes. *Phytochem Rev.* **70**, 1522-1531.
18. Jefoate, C. R. E. and Gaylor, J. L. (1969) Ligand interactions with hemoprotein P-450. II. Influence of phenobarbital and methylcholanthrene induction processes on P-450 spectra. *Biochemistry* **8**, 3464-3472.
19. Song, W. C. and Brash, A. R. (1991) Purification of an allene oxide synthase and identification of the enzyme as a cytochrome P-450. *Science* **253**, 781-784.
20. Locuson, C. W., Hutzler, J. M. and Tracy, T. S. (2007) Visible spectra of type II cytochrome P450-drug complexes: evidence that "incomplete" heme coordination is common. *Drug. Metab. Dispos.* **35**, 614-622.
21. Agrawal, G. K., Tamogami, S., Han, O., Iwahashi, H. and Rakwal, R. (2004) Rice octadecanoid pathway. *Biochem. Biophys. Res. Commun.* **317**, 1-15.
22. Agrawal, G. K., Rakwal, R., Jwa, N. S., Han, K. S. and Agrawal, V. P. (2002) Molecular cloning and mRNA expression analysis of the first rice jasmonate biosynthetic pathway gene allene oxide synthase. *Plant Physiol. Biochem.* **40**, 771-782.
23. Ha, S. B., Lee, B., Lee, D. E., Kuk, Y. I., Lee, A. Y., Han, O. and Back, K. (2002) Molecular characterization of the gene encoding rice allene oxide synthase and its expression. *Biosci. Biotechnol. Biochem.* **66**, 2719-2722.
24. Kim, E. S., Choi, E., Kim, Y., Cho, K., Lee, A., Shim, J., Rakwal, R., Agrawal, G. K. and Han, O. (2003) Dual positional specificity and expression of non-traditional lipoxygenase induced by wounding and methyl jasmonate in maize seedlings. *Plant Mol. Biol.* **52**, 1203-1213.
25. Jang, S., Huon, T., Kim, K., Um, E. and Han, O. (2007) Regiochemical and stereochemical evidence for enzyme-initiated catalysis in dual positional specific maize lipoxygenase-1. *Org. Lett.* **9**, 3113-3116.
26. Oh, K. and Murofushi, N. (2002) Design and synthesis of novel imidazole derivatives as potent inhibitors of allene oxide synthse (CYP74). *Bioorg. Med. Chem.* **10**, 3707-3711.
27. Wasternack, C. and Kombrink, E. (2010) Jasmonates: Structural requirements for lipid-derived signals active in plant stress responses and development. *ACS Chem. Biol.* **5**, 63-77.
28. Hoa, G. H. B., Primo, C. D., Geze, M., Douzou, P., Kornblatt. J. A. and Sligar, S. G. (1990) The formation of cytochrome P-450 from chtochrome P-420 is promoted by spermine. *Biochemistry* **29**, 6810-6815.
29. Vick, B. A. (1991) A spectrophotometric assay for hydroperoxide lyase. *Lipids* **26**, 315-320.
30. Cho, K. B., Lai, W., Hamberg, M., Raman, C. S. and Shaik, S. (2011) The reaction mechanism of allene oxide synthase: Interplay of theoretical QM/MM calculations and experimental investigations. *Arch. Biochem. Biophys.* **507**, 14-25.